

Stable ultrahigh-density magneto-optical recordings using introduced linear defects

L. Krusin-Elbaum^{*†}, T. Shibauchi^{*†§}, B. Argyle^{*}, L. Gignac^{*} & D. Weller^{‡||}

^{*}IBM T. J. Watson Research Center, Yorktown Heights, NY 10598, USA

[§]MST-STC, Los Alamos National Laboratory, MS-K763, Los Alamos, NM 87545, USA

[‡]IBM Almaden Research Center, San Jose, CA 95120, USA

[†]These authors contributed equally to this work

The stability of data bits in magnetic recording media^{1,2} at ultrahigh densities is compromised by thermal ‘flips’ – magnetic spin reversals – of nano-sized spin domains³, which erase the stored information. Media that are magnetized perpendicular to the plane of the film, such as ultrathin cobalt films or multilayered structures^{4,5}, are more stable against thermal self-erasure^{2,6} than conventional memory devices. In this context, magneto-optical memories seem particularly promising for ultrahigh-density recording on portable disks, and bit densities of ~ 100 Gbit inch⁻² (ref. 7) have been demonstrated using recent advances in the bit writing and reading techniques^{7–11}. But the roughness and mobility of the magnetic domain walls^{12,13} prevents closer packing of the magnetic bits, and therefore presents a challenge to reaching even higher bit densities. Here we report that the strain imposed by a linear defect in a magnetic thin film can smooth rough domain walls over regions hundreds of micrometers in size, and halt their motion. A scaling analysis of this process, based on the generic physics of disorder-controlled elastic lines^{14–17}, points to a simple way by which magnetic media might be prepared that can store data at densities in excess of 1 Tbit inch⁻².

Increasing information storage to densities past 100 Gbit inch⁻² may evolve through extensions of current magnetic recording technologies (to patterned media⁶, for example). But such increases in storage density might be achieved by using other techniques such as holography (via interference patterns produced by two intersecting laser beams)¹⁸, or micromachined nano-cantilever arrays¹⁹, or – to satisfy a relentless demand for portability – using scanning localized subwavelength ($< \lambda/40$) (near-field) optical probes⁹ that can imprint and resolve images in magneto-optic media⁸ of the order of the probe size. The bit-writing with local probes may be thermally assisted by a current²⁰ or a laser beam that raises local temperature to the vicinity of the Curie temperature T_C , resulting in the formation of a reversed domain with a rough wall. To realize smooth and (for precise positioning) stable (‘noiseless’) domain walls that can be implemented without, for example, nanoscale patterning, we suggest a conceptual identification of walls with elastic lines¹⁶ and seek to utilize linear defects inducing a direc-

tional long-range strain field in ultrathin Pt/Co/Pt structures – long considered excellent candidates for high-density recording at blue-range wavelengths¹¹. In such trilayers (Fig. 1), large uniaxial perpendicular anisotropy is sustained by the interface contribution $\propto 1/d_{\text{Co}}$ up to Co thickness $d_{\text{Co}} \sim 1.5$ nm; beyond this thickness the magnetization switches from out-of-plane to in-plane⁵.

Figure 2a shows two typical up-domains (see legend for imaging details²¹), nucleated owing to a locally suppressed coercive field³ H_c in a 0.7 nm Co film sandwiched between 3 nm (top) and 2 nm (bottom) Pt layers, prepared using standard deposition parameters²² and without linear defects. The domains are round with (undirected) domain walls (DWs) that are as rugged as expected¹². We note that patterned nucleation sites, as in Fig. 2b-d, do not reduce either DW roughness or velocity. As magnetic field is increased beyond $H_c = 750$ Oe (inset in Fig. 3), the outward motion of DWs becomes increasingly swift (estimated from displacement of a small segment of the wall during 500-ms field pulses, the wall velocity is more than $180 \mu\text{m s}^{-1}$ at $H = 854$ Oe).

To control the rugged DW structure we will use a recently found connection between the DW behavior in thin films¹³ and that of elastic lines^{14–16}. One prominent example of directed elastic lines are wandering vortex lines (quantized magnetic flux lines maintained by a swirling tube of current) in high temperature superconductors¹⁶ that can be strongly localized by interaction with columnar (linear) defects¹⁷. A powerful arsenal of ideas can now be engaged to understand how a linear defect potential may localize and reduce the roughness of DWs, and force them to accommodate to the defect shape. We introduce a line defect that delivers a three-punch action. Through magneto-elastic coupling, (i) it gives the wall a preferred direction¹⁴ (along the defect), (ii) it increases its elasticity, reducing the DW roughness as it negotiates the random landscape, and (iii) it acts to reduce wall velocity to a nearly full stop in fields greater than the coercive field of unmodified film. The defect is installed during the Co deposition by imposing an anisotropic tension (clamping) on the substrate and its subsequent release²³. The resulting Co ‘fold’ (Fig. 2g,h) introduces a y -axis invariant long-range strain field $\varepsilon(x)$.

A DW driven by the magnetic field toward such linear defect (Fig. 2e,f) presents a structural contrast with the DWs in the unmodified film in Fig. 2a. Even at large distances ($\sim 300 \mu\text{m}$) away from the defect, the

DW conforms on the average to the defect line along y . It becomes progressively smoother (and straighter) as it approaches the defect. It also rapidly decelerates. The deceleration and near-standstill of the wall depends on the proximity to the defect, as represented by the spatial progression of the velocity-versus-field (force) response in Fig. 3. The v - H curves are highly nonlinear, as has been reported recently in Co films¹³ where the disorder landscape is formed, for example, by atomic scale imperfections at the film-substrate interface. Such nonlinear response in the limit of vanishing driving force is a signature of glassy (creep) dynamics²⁴, well established for the elastic vortex lines in a superconductor through measurements of the voltage-versus-current (V - I) characteristics¹⁶. Above H_{crit} (obtained from the v - H curves by the usual velocity cut-off criterion, here chosen at $v = 0.14 \mu\text{m s}^{-1}$) the driving field exceeds the ‘pinning’ force¹⁶ and the DW response becomes linear and faster. We note that DW velocity, even far away from a line defect, is orders of magnitude lower than in unmodified films. Figure 3 shows a field-forward advance of v - H curves to higher fields, and an enhanced H_{crit} (often referred to as a ‘propagation field’³) on the approach to the line defect. An effective potential well that localizes the wall is formed by the driving field pushing the wall and the line-defect that acts against this push. It resembles columnar defects in a superconductor, where the critical current J_{crit} is enhanced¹⁷. H_{crit} correlates with the long-range repelling force field $H(x)$ exerted on the DWs by the line-defect, whose spatial extent is mapped in Fig. 4a. The shape of $H(x)$ – a ridge along y – is either extracted directly from Kerr images taken with increasing H after a fixed propagation time t (main panel), or more quantitatively from the averaged DW positions $\langle x \rangle_y$ versus time at all fields. As illustrated in the inset, it takes a higher field H to get closer to the line-defect; but at any H , after $t = 1,800$ s, two DWs – one approaching the ridge from the left and another from the right – become effectively stationary.

Within the elastic description of a DW, the relevant scale is a collective pinning²⁴ length $L_c = (\epsilon_{el}^2 \xi^2 / \Delta)^{1/3}$, where ξ and Δ are characteristic size and strength of underlying random disorder, and ϵ_{el} is the wall energy. At lengths $L > L_c$, the wall will elastically adjust to the random landscape to nestle in a local minimum energy configuration. The DW energy density (in addition to a uniform field term and ignoring a weak dipolar term) can be written as a sum of three: the exchange energy $\gamma_{ex}(x)$, the anisotropy energy $\gamma_{an}(x)$, and the magneto-elastic energy²⁵ $\gamma_{m-el}(x)$ coupling to the strain $\varepsilon(x)$ generated by the line-defect,

$$\gamma_{DW} = \underbrace{A(d\theta/dx)^2}_{\gamma_{ex}} - \underbrace{K'm_z^2}_{\gamma_{an}} - \underbrace{B\varepsilon(x)m_z^2}_{\gamma_{m-el}} + H^2/8\pi. \quad (1)$$

Here A is the exchange stiffness³, $K' = K - 2\pi M_S^2$ (K is the anisotropy constant and M_S is Pt-polarization-

enhanced saturation magnetization of Co), and B is related to Young’s modulus of the film. Magnetization \vec{M} rotates from ‘up’ to ‘down’ within the wall thickness δ (we estimate at ~ 3 nm) and the wall (in the simplest form) is of Bloch type¹³, where the azimuthal angle $\phi = 0^\circ$ and the rotation is parameterized by an angle θ between the z -axis and \vec{M} (m_z is the direction cosine along z). Minimizing $\int \gamma_{DW} dx$ leads to DW energy³

$\mathcal{E}_{DW} = 4\sqrt{AK'_{eff}}$, where $K'_{eff} = K' + B\varepsilon(x)$. The total wall energy (per unit area) in a magnetic field H is $\mathcal{E} = \mathcal{E}_{DW} - 2M_S Hx$. From the stability condition $d\mathcal{E}/dx = 0$ we obtain a nonlinear differential equation for $\varepsilon(x)$: $H(x) = AM_S^{-1}B(d\varepsilon/dx)(AK'_{eff})^{-1/2}$, which we solve numerically using the stationary $H(x)$ mapped in Fig. 4a. The result is a factor of ~ 2 enhanced effective anisotropy K'_{eff} (Fig. 4b) and, consequently, an enhanced DW elastic energy (per unit length)¹³ $\epsilon_{el} = 4\sqrt{AK'_{eff}}d_{Co}$. Thus, the enhanced elasticity of DW is in part responsible for the longer L_c . The longer L_c is a key to the reduced DW roughness. This can be seen from the analysis of transverse displacements of the domain wall segments by computing from the DW images a (line shape) correlator¹⁴ $x_t = \sqrt{\langle [x(y) - x(y+L)]^2 \rangle}$, predicted for $L < L_c$ to scale as¹⁶ $x_t \propto (L/L_c)^{3/2}$. We find that the characteristic length L_c is enhanced in the vicinity of the line-defect by a factor of ~ 5 (Fig. 4c). This implies a reduction of roughness, as measured by x_t , by a factor of ~ 10 on the shortest length scales and hence a potential increase in the areal density by nearly two orders of magnitude. In its proximity, the line defect wins over randomness so that on sufficiently long distances along its length DWs become essentially ‘flat’ (that is, finite x_t for $L \rightarrow \infty$)¹⁴ in fields up to $\sim 2H_c$. The wall-smoothing at higher fields and at speeds of current recording technology ($H \approx 3H_c$, ~ 1 Gbit s^{-1}) deserves further study for practical implementations of this effect. The long-range strain associated with a line defect presents an efficient, and relatively simple and cost-effective control of domain walls, with only a few such defects needed to stabilize large areas of ultrathin films.

¹ *Magnetic Recording: The First Hundred Years*. Eds. Daniel, E.D., Mee, C.D. & Clark, M.H. (IEEE Press, New York, 1998).

² Thompson, D.A. & Best, J.S. The future of magnetic data storage technology. *IBM J. Res. Develop.* **44**, 311-322 (2000).

³ Hubert, A. & Schäfer, R. *Magnetic domains* (Springer, New York, 1998).

⁴ Kirby, R.D., Shen, J.X., Hardy, R.J. & Sellmyer, D.J. Mag-

- netization reversal in nanoscale films with perpendicular anisotropy. *Phys. Rev. B* **65**, R10810-13 (1994).
- ⁵ Allenspach, R., Stampanoni, M. & Bischof, A. Magnetic domains in thin epitaxial Co/Au(111) films. *Phys. Rev. Lett.* **65**, 3344-47 (1990).
- ⁶ Weller, D. & Moser, A. Thermal effect limits in ultrahigh density magnetic recording. *IEEE Trans. Magn.* **35**, 4423-39 (1999).
- ⁷ Partovi, A. Optical near-field aperture storage technique for high density, high performance data storage applications. *SPIE* **3864**, 352-354 (1999).
- ⁸ Awano, H. & Ohta, N. Magneto-optical recording technology toward 100 Gb/in². *IEEE J. Selected Topics in Quantum Electronics* **4**, 815-820 (1998).
- ⁹ Betzig, E., Trautman, Harris, T.D., Weiner, J.S. & Kostelak, R.L. Breaking the diffraction barrier: optical microscopy on a nanometer scale. *Science* **251**, 1468-1470 (1991).
- ¹⁰ Partovi, A. *et al.* High-power laser light source for near-field optics and its application to high-density optical data storage. *Appl. Phys. Lett.* **75**, 1515-17 (1999).
- ¹¹ Kaneko, M. Magnetic multilayer films for high density magneto-optical recording. *J. Magn. Magn. Mater.* **148**, 351-356 (1995).
- ¹² Han, S.K, Yu, S.-C. & Rao, K.V. Domain wall jaggedness induced by the random anisotropy orientation in magneto-optic materials: A computer simulation study. *J. Appl. Phys.* **79**, 4260-64 (1996).
- ¹³ Lemerle, S. *et al.* Domain wall creep in an Ising ultrathin magnetic film. *Phys. Rev. Lett.* **80**, 849 (1998).
- ¹⁴ Halpin-Healy, T. & Zhang, Y.-C. Kinetic roughening phenomena, stochastic growth, directed polymers and all that. *Phys. Rep.* **254**, 215-414 (1995).
- ¹⁵ Hwa, T. From vortices to genomics. *Nature* **399**, 17-18 (1999).
- ¹⁶ Blatter, G., Feigel'man, M. V., Geshkenbein, V. B., Larkin, A. I. & Vinokur, V. M. Vortices in high-temperature superconductors. *Rev. Mod. Phys.* **66**, 1125 (1994).
- ¹⁷ Krusin-Elbaum, L. *et al.* Superconductivity enhanced by Hg fission. *Nature* **389**, 243-244 (1997).
- ¹⁸ Heanue, J.F., Bashaw, M.C. & Hasselink, L. Volume holographic storage and retrieval of digital data. *Science* **265**, 749-752 (1994).
- ¹⁹ Binnig, G.K., Rohrer, H. & Vettiger, P. Mass-storage applications of local probe arrays. *U.S. Patent 5,835,477*, November 10, 1998.
- ²⁰ Nakamura, J., Miyamoto, M., Hosaka, S. & Koyanagi, H. High-density thermomagnetic recording method using a scanning tunneling microscope. *J. Appl. Phys.* **77**, 779-81 (1995).
- ²¹ Argyle, B.E. & McCord, J.G. New laser illumination method for Kerr microscopy. *J. Appl. Phys.* **87**, 6487- 6489 (2000).
- ²² Weller, D. *et al.* Ion induced magnetization reorientation in Co/Pt multilayers for patterned media. *J. Appl. Phys.* **87**, 5768-70 (2000).
- ²³ Deng, H., Jarratt, J.D., Minor, M.K. & Barnard, J.A. Artificially controlled stress anisotropy and magnetic properties of FeTaN thin films. *J. Appl. Phys.* **81**, 4510-12 (1997).
- ²⁴ Feigel'man, M. V., Geshkenbein, V. B., Larkin, A. I. & Vinokur, V. M. Theory of collective flux creep. *Phys. Rev. Lett.* **63**, 2303-2306 (1989).
- ²⁵ Chuang, D.S., Ballentine, C.A. & O'Handley, R.C. Surface and step magnetic anisotropy. *Phys. Rev. B* **49**, 15084-15095 (1994).

Acknowledgements

We thank J. Slonczewski, V. Vinokur, G. Blatter, and G. Zimanyi for useful discussions. Correspondence and requests for materials should be addressed to L. Krusin-Elbaum, fax: +1-914-945-2141; e-mail: krusin@us.ibm.com.

^{||} present address: Seagate Technology, Pittsburgh, PA 15203, USA.

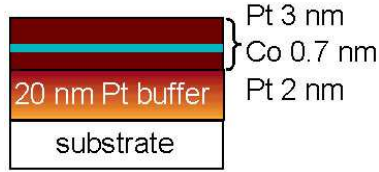


FIG. 1. A sketch of an ultrathin Pt/Co/Pt trilayer stack explored in this study. Stacks were electron-beam evaporated at 190°C on glass or SiN_x/Si substrates with a 20 nm (111) textured Pt buffer layers, as described in ref. 22.

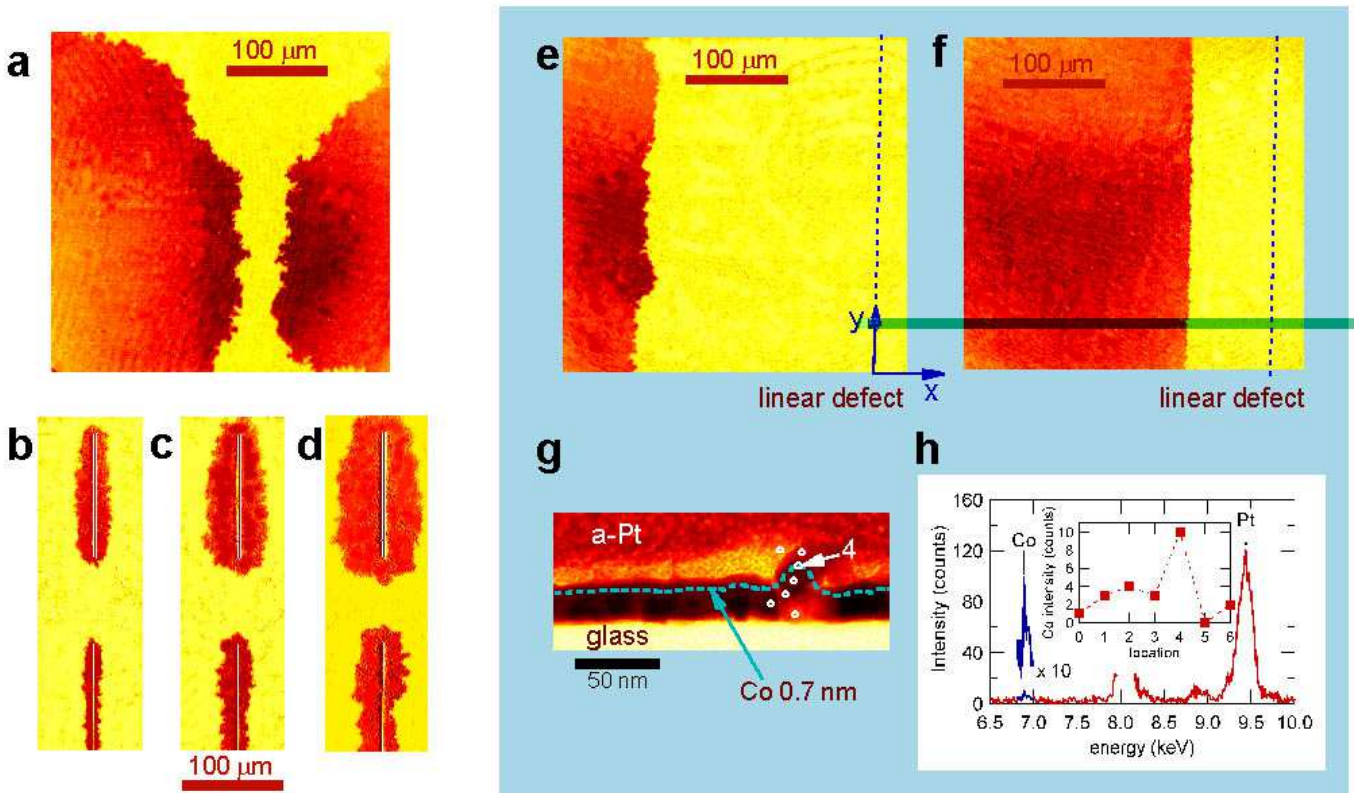


FIG. 2. Effect of a linear defect on domain walls in Pt/Co/Pt films. Polar magneto-optic Kerr microscopy³ images were obtained using a 3-W argon laser illumination ($\lambda = 514.5$ & 488.0 nm) to enhance phase contrast with a laser-beam tandem-dithering technique²¹ to eliminate the effects of laser coherence. We first saturated magnetization with a negative z -axis magnetic field and then quenched field to zero. After a first positive square field pulse, an up-domain was nucleated and its motion was imaged at short time intervals in fields up to ~ 2 kOe. **a**, Typical room-temperature image of domains in a film without line defects after a 854-Oe magnetic field applied for 1 s was removed. The walls show roughness on length scales much larger than the grain size (~ 20 -30 nm) of the Pt buffer. The rapid motion of domain walls (DWs) is illustrated in snapshots in field $H = 616$ Oe after **b** 1 s, **c**, 4 s and **d**, 8 s of DWs that were seeded with elongated defects installed with a 30-keV Ga⁺ FIB (Focused Ion Beam). DW roughness is independent of the seed-defect width (150 nm for bottom and 1 μ m for top domains). **e**, **f**, A remarkable reduction in the domain wall roughness and speed is illustrated when a line-defect (dashed line along y axis) is introduced. The images here were taken at $H = 924$ Oe ($> H_c = 750$ Oe in **a**) at **e**, 40 s and **f**, 1,800 s. The domain wall becomes directed along the defect. A cross-sectional electron transmission micrograph (**g**) of an ~ 30 -nm-thin FIBed section – normal to the line-defect – shows an asymmetric ‘fold’ of the trilayer stack. An amorphous Pt (a-Pt) cap was deposited to protect the trilayer during the FIB process. The ~ 10 -nm elevation of Co in the ‘fold’ is traced by the X-ray microprobe (**h**) at spots such as are marked by six white circles in **g** (the bottom is assigned ‘0’). Co intensity versus spot number is plotted in the inset of **h**.

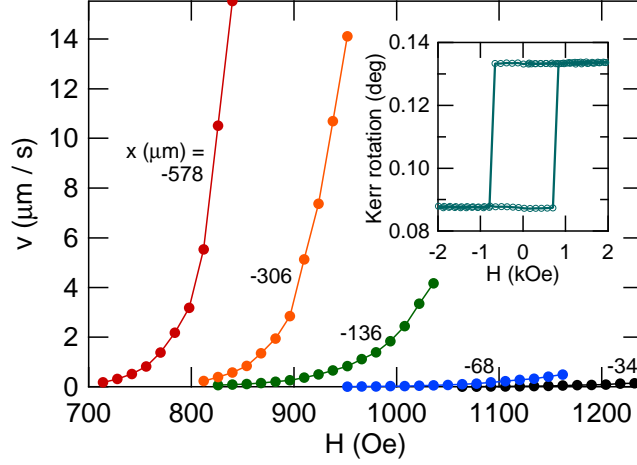


FIG. 3. Domain wall velocity as a function of applied magnetic field for different values of x . Far away ($-578 \mu\text{m}$) from the line-defect ‘ridge’ at $x = 0$, the velocity takes off rapidly with field near H_{crit} . Well below H_{crit} , the nonlinear v - H curves follow¹³ $v(H) \propto \exp[-(U_c/k_B T)(H_{crit}/H)^\mu]$, where U_c is the collective pinning energy scale, k_B is the Boltzmann constant, T is temperature, and $\mu = 1/4$ is the glassy dynamical exponent related to the roughness exponent, see ref. 14. H_{crit} grows on the approach to the line defect (see Fig. 4a). Inset: A square Kerr rotation (magnetization) hysteresis characteristic of perpendicular anisotropy of our film in Fig. 2a.

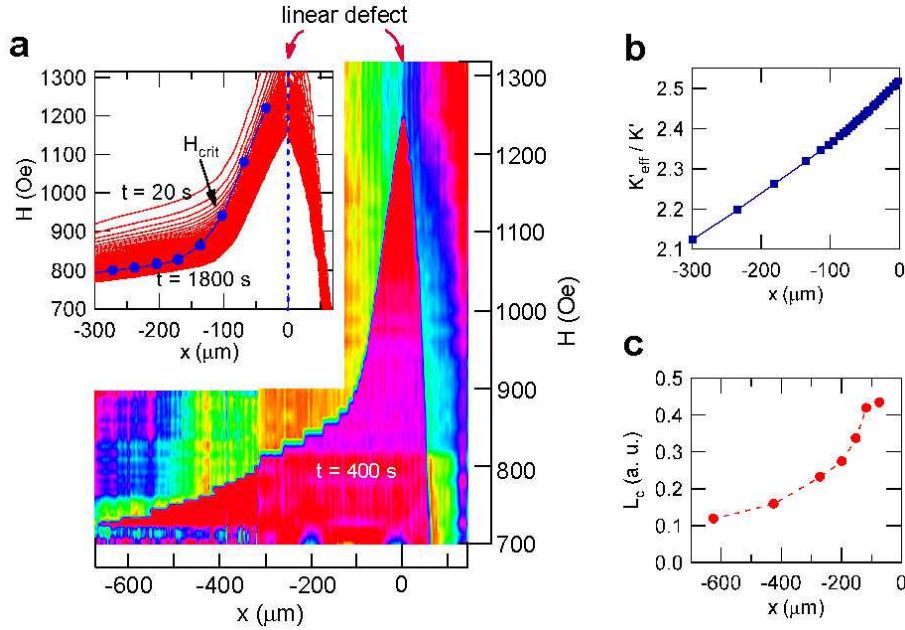


FIG. 4. A force field $H(x)$ generated by a line-defect along y repels a magnetic-field-driven domain wall. **a**, A fixed y -cut from a map of the defect ridge obtained from combining domain images for different fields after 400 s. To display the long range ($x = -680$ to $+140 \mu\text{m}$) of the force field of the line defect, we overlapped two series of Kerr observations ($H = 700$ to $1,316$ Oe): one containing a line defect at $x = 0$ (as in the inset) and another shifted to the left by $400 \mu\text{m}$. The ridge is mapped by imaging two domains approaching it from both sides. Contours (at 20-s intervals) of the defect field (inset) that were obtained by extracting DW positions at different times and fields show how two DWs on two sides of the ridge become stationary when defect field balances the driving field, defining the ridge’s outline. The propagation field H_{crit} (solid blue dots), obtained from v - H curves in Fig. 3 is enhanced by the line defect. The line defect effectively enhances **(b)** the anisotropy constant K'_{eff} and elongates **(c)** the scaling length L_c .